Composites Science and Technology 135 (2016) 137–145

Contents lists available at ScienceDirect

Composites Science and Technology

journal homepage: http://www.elsevier.com/locate/compscitech

Enhanced mechanical properties of polyimide composite fibers containing amino functionalized carbon nanotubes

Jie Dong, Yuting Fang, Feng Gan, Jinyin An, Xin Zhao, Qinghua Zhang*

State Key Laboratory for Modification of Chemical Fibers and Polymer Materials, College of Materials Science and Engineering, Donghua University, Shanghai 201620, PR China

ARTICLE INFO

Article history:
Received 25 July 2016
Received in revised form
22 September 2016
Accepted 22 September 2016
Available online 22 September 2016

Keywords:
NH_2-MWCNTs
Polyimide composite fiber
Interfacial interaction
Hydrogen-bonding
Aggregation structure

ABSTRACT

Carbon nanotubes (CNTs) have been gained attention and interest to be as ideal reinforcement fillers due to their exceptional theoretical mechanical properties for a long time. To date, the reinforcing effect of the CNTs in most composite systems is still not satisfied. In the present study, by incorporating a novel NH_2-MWCNTs/NMP suspension into the polyimide matrix *in situ* polymerization, a series of PI/NH_2-MWCNTs composite fibers have been fabricated using wet-spinning technique. Detailed studies based on different spectroscopic characterizations suggested that there exist multiple interfacial interactions between NH_2-MWCNTs and polyimides (PIs) including the hydrogen bonding and π-π interaction. Wide-angle X-ray scattering measurements revealed the evolution of the aggregation structure of these composite fibers during heat-drawing process, and the results illustrated that the incorporated amino functionalized CNTs showed beneficial effects on the packing and orientation of PI molecular chains. Attributed to the above advantages, the resulting composite fiber containing 0.4 wt% NH_2-MWCNTs presented a tensile strength of 2.41 GPa (approximately a 47% increase over neat PI fiber), and the modulus of 99 GPa (27% raises compared with neat PI fiber). Meanwhile, dimensional stability of the PI fibers also has been improved by this effective approach.

1. Introduction

Aromatic polyimide fiber (PI) has been recognized as one of the most important high-performance polymeric fibers with superior performances such as excellent thermal stability, good chemical resistance, radiation shielding capability and so on [1–3]. In order to expand the application of the PI fibers, mechanical properties and other performance need to be improved. Generally, there are two approaches to improve the mechanical properties of PI fibers: to structurally modify the aromatic PIs and to fabricate PI-based composites with reinforcements. For the structure modification, such as introducing rigid heterocyclic units to the polymer backbones, several researchers have made great efforts. Sukhanova et al. fabricated a series of high performance PI fibers containing the rigid aromatic diamine 2,5-bis(4-aminophenyl)-primidine (PRM) with a tensile strength and modulus of 3.0 and 130 GPa, respectively [4]. Niu and the co-workers introduced the rigid monomer 2-(4-aminophenyl)-6-amino-4(3H)-quinazolinone (AAQ) into the PI chains and the strength and modulus of the fibers were up to 2.8 GPa and 115 GPa, respectively [5]. Even though the mechanical properties of the PI fibers have been improved by introducing rigid heterocyclic units into the polymer chains, concomitantly, shortcomings are still followed: these monomers currently are not widely available or highly expensive. PI fiber reinforcement using a nanofiller is another promising way to improve the tensile properties as well as expand their applications [6–8]. In recent years, more and more nanomaterials with remarkable properties have been introduced into polymer matrices to modify the inadequacies of the materials to meet the stringent requirements under some special circumstances [9–12]. Among these candidates, carbon nanotubes (CNTs) have gained intensive attention as one of the most promising reinforcement nanomaterials due to their extraordinary mechanical properties, high aspect ratio and excellent thermal stability [13–15]. Introducing CNTs into polymeric fibers has been widely utilized and investigated over the past decades [16]. However, the tensile strength and modulus of these composite fibers just reached a small fraction of the theoretical value, and some polymer/CNTs systems even showed decreased tendency of mechanical properties when incorporating CNTs into the polymer matrix [17,18], which were mainly attributed to the

* Corresponding author.
E-mail address: qhzhang@dhu.edu.cn (Q. Zhang).

http://dx.doi.org/10.1016/j.compscitech.2016.09.021
0266-3538/

dispersion difficulties and poor interaction between the polymer matrix and CNTs. Therefore, a key issue for raising the reinforcement of nanofillers includes improving both the homogeneous dispersion and interfacial interaction between the polymer and CNTs. Recently, great efforts have been focused on applying the approach of surface modification of CNTs to improve the compatibility between the matrix and the nanofillers. Hu et al. found that the incorporation of CNT-COOH into the poly (*p*-phenylene benzobisoxazole) (PBO) matrix by one-pot *in situ* polycondensation increased the tensile strength and modulus of PBO fiber from 2.2 to 2.7 GPa and from 64.8 to 89.4 GPa [19]. Sainsbury et al. functionalized MWCNTs with poly (*p*-phenylene terephthalamide) (PPTA) oligomer units, which facilitates the integration of the PPTA-MWCNTs within the PPTA matrix [20].

In this work, the asymmetric heterocyclic diamine 2-(4-aminophenyl)-5-aminobenzimidazole (BIA) and the rigid-rod dianhydride 3,3′,4,4′-biphenyltetracarboxylic (BPDA) were selected to synthesize the PI. Meanwhile, amino-functionalized MWCNTs as reinforcement fillers were introduced into PI matrix expecting enhancing the fibers' mechanical and other performances. In general, properties of polymeric fibers mainly depend on the aggregation structure and intermolecular interactions [5,21,22]. The orientation of the molecule chains as well as the formation of the interfacial interactions can be affected by the incorporated CNTs, especially when forming extra interactions or covalent bonds between polymer matrix and functional groups on the surfaces of the CNTs, thus leading to the changes of the performances of the fibers [15,17,23]. However, until now, less systematic studies have focused on investigating the interactions between CNTs and PI chains, polymer chains orientation as well as the semicrystalline structure of PI/CNTs composite fibers. Herein, we report a new effective protocol to prepare PI/CNTs composites on the basis of NH_2-MWCNTs/NMP suspensions by *in situ* polymerization to improve the solubility, dispersivity and interfacial interactions of CNTs in the PI matrix. A series of PI/NH_2-MWCNTs composite fibers were prepared by wet-spinning process and post heat-drawing treatment. Intricate interactions between CNTs and PI as well as the evolution of the aggregation structure of the composite fibers were investigated intensively and correlated to the mechanical and other performances of the prepared composite fibers.

2. Experimental section

2.1. Materials

MWCNTs with the CNTs' diameter of 10–20 nm and a length of 10–20 μm was supplied by Time Nano Co. Ltd, China. The amino functionalized NH_2-MWCNTs and NH_2-MWCNT/NMP suspensions were prepared according to the previous works [24,25]. The content of amino group (–NH_2) on the surface of MWCNTs was around 0.45 wt%. 3,3′,4,4′-Biphenyltetracarboxylic dianhydride (BPDA, 99.5%) was purchased from Shijiazhuang Haili Pharmaceutical Co., Ltd. and was purified *via* sublimation under reduced pressure. 2-(4-aminophenyl)-5-aminobenzimidazole (BIA) was supplied by Zhejiang Dragon Chemical Group Co., Ltd. *N*-methyl-2-pyrrolidone (NMP) was purchased from Adamas Chemicals and purified by distillation prior to use. Kevlar 29 and Kevlar 49 fibers was purchased from Dupont, USA. PBO fibers was supplied by the State Key Laboratory For Modification of Chemical Fibers and Polymer Materials, China.

2.2. Synthesis of poly(amic acid) (PAA)/NH_2-MWCNTs spinning dopes

PAA/NH_2-MWCNTs spinning dopes with various loadings of NH_2-MWCNTs were synthesized by the following procedure as shown in Scheme 1(A). A representative polymerization is as follows: A 250 mL three-necked flask equipped with a nitrogen inlet and a mechanical stirrer was charged with distilled NMP, BIA (11.21 g, 0.05 mol) and appropriate amount of NH_2-MWCNTs/NMP suspensions. Equimolar dianhydride BPDA (14.711 g, 0.05 mol) was added as the diamine was dissolved. The solution was stirred at a low temperature (0–5 °C) for 12 h. Thus a series of spinning solutions with different NH_2-MWCNTs loadings (0, 0.1, 0.2, 0.4, 0.8 wt %) were obtained and kept in a freezer until use.

2.3. Preparation of composite fibers

The obtained spinning solutions were degassed at room temperature prior spinning. The precursor PAA/NH_2-MWCNTs composite fibers were fabricated *via* extruding the composite dopes through a spinneret (50 holes with 80 μm in diameter) into a coagulation bath (pure water), as shown in Scheme 1(B). Solidified filaments entered into the following washing bath. Then, the precursor fibers were dried under vacuum at 60 °C for 12 h, and then converted to polyimide fibers by successive heating at 100, 200 and 300 °C for 1 h at each temperature. Finally, the PI/NH_2-MWCNTs composite fibers were drawn with various ratios in a furnace over 430 °C.

2.4. Characterization

Viscosities of the spinning solutions were characterized with a MCR 301 rheometer. Morphologies of the fibers were observed on a scanning electron microscope (SEM) (HITACHI SU8010) at an accelerating voltage of 3.0 kV. ATR-FTIR spectra were recorded on a Nicolet 8700 spectroscope with the range of 4000–400 cm^{-1}. X-ray photoelectron spectroscopy (XPS) experiments were carried out on a PHI 5000C ESCA System using a monochromatic Al X-ray source (987.9 W, 1486.6 eV). Data analysis was carried out using CasaXPS software. Two-dimensional wide angle X-ray diffraction (WAXD) profiles were obtained at Beamline 16 B1 in the Shanghai Synchrotron Radiation Facility (SSRF). The wavelength is 0.775 nm. A CCD X-ray detector (MAR CCD 165) was employed at a distance of 168.5 mm from the sample for WAXD measurement. A typical image acquisition time was 40 s. The scattering patterns were analyzed using the software package x-Polar. Mechanical properties of the composite fibers were measured with the XQ-1 instrument, and the loading rate and gauge length are 10 mm/min and 15 mm, respectively. One specimen was measured at least ten times and the average value was used as the representative. Thermal stability of the fibers was analyzed using a Netzsch 209 F3 under nitrogen flow. Thermal dynamic mechanical behavior of the composite fibers was carried out on a thermomechanical analyzer (TA, Q800) from 50 to 550 °C at a heating rate of 3 °C/min. Thermal dimensional stability of the composites was also tested on Q800 under a tension force of 8 MPa.

3. Results and discussion

Fig. 1 shows the dependence of viscosities of the PAA/NH_2-MWCNTs spinning solutions with various CNTs mass fractions on the shear rates. Clearly, at relatively low shear rate, an increase in nanotube loadings from 0 to 0.4 wt% leads to a continuous increase of the viscosity η_a, ranging from 100 Pa s to 400 Pa s, which is due to the effect of NH_2-MWCNTs. Increasing the CNTs loading further to 0.8 wt% results in a decrease in the shear viscosity, attributing to the obstacle effect of NH_2-MWCNTs on the molecule weights of PAAs. Actually, the increased viscosities endow the spinning dopes with better spinnability, which has been observed in the spinning

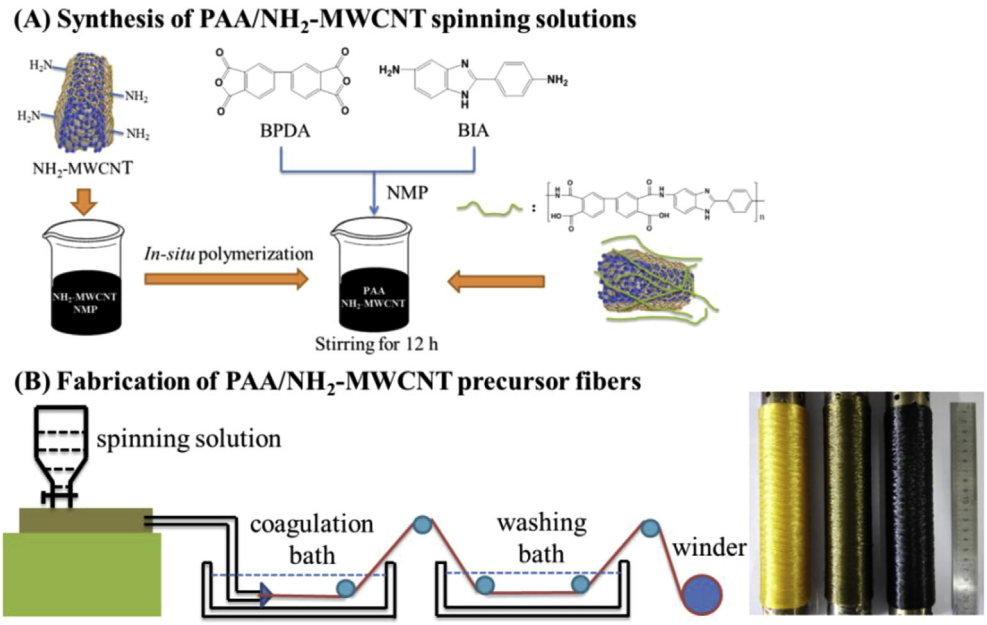

Scheme 1. Schematic synthesis of PAA/NH_2-MWCNTs spinning solutions (A) and fabrication of precursor composite fibers *via* wet-spinning process (B).

process. As an interesting phenomenon, the presence of NH_2-MWCNTs reduces the linear viscoelastic region of the PAA matrix, especially at high loading levels.

The precursor composite fibers were spun by a wet-spinning method. The construction of interfacial regions with strong interactions is an essential condition for the achievement of improved mechanical properties within composites. High-resolution SEM images of cryogenic fractured surfaces of composite fibers with nanotube contents of 0, 0.4 and 0.8 wt% are shown in Fig. 2. The neat PAA fiber shows dense as well as uniform morphology. For other samples, nanotubes are dispersed homogeneously throughout the cross-section of the fiber without obvious aggregates, which are mainly benefitted from the utilization of NH_2-MWCNTs/NMP suspensions. Meanwhile, some nanotubes were partially pulled out from the matrix's cross-section (indicated by the red arrows), but most nanotubes were broken on the cross-sections and well wetted by the polymer matrix (indicated by the blue arrows), suggesting the strong polymer-nanotube interfacial adhesion, which was beneficial for their good mechanical properties.

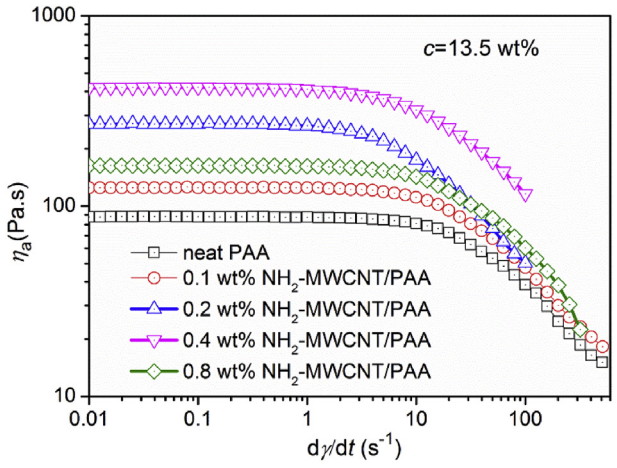

Fig. 1. Steady state shear viscosity of PAA/NH_2-MWCNTs/NMP solutions with various CNT mass fractions used for fiber spinning.

Chemical structures of the NH_2-MWCNTs, neat PI and composite fibers were characterized by ATR-FTIR as shown in Fig. 3(A). It is clearly shown that two bands at 1226 and 1640 cm^{-1} appear in the spectra for NH_2-MWCNTs, which are assigned to the carbonyl groups (amide C═O) and C–N groups. A broad band at 3500–3200 cm^{-1} can be assigned to the amino groups. Apparently, all composite fibers exhibit typical characteristic imide peaks at 1780 cm^{-1} (imide C═O symmetric stretching), 1720 cm^{-1} (imide C═O asymmetric stretching) and 1370 cm^{-1} (C–N stretching), respectively, illustrating the complete imidization from the precursor fibers to PI/NH_2-MWCNTs composite fibers. Interestingly, as shown by the local enlarged FTIR spectra in Fig. 3(B), upon the addition of NH_2-MWCNTs, the carbonyl band around 1720 cm^{-1} shifts to lower wavelength numbers, which indicates the formation of hydrogen bonding interactions [26,27]. For these composites, the carbonyl bands in the matrix (polyimide) are expected to offer appropriate condition for the forming hydrogen bonding interaction with richful NH_2 groups on the surface of the nanotubes. Zhu and the co-workers have also illustrated the existence of hydrogen bonding interactions between the Kevlar nano-fiber and acid-treated carbon nanotubes, which play an important role in reinforcing the composites' mechanical properties [15].

We further tried to use Raman spectroscopy to evaluate other possible interactions between the matrix and the nano fillers. Unfortunately, it is hard to identify the obvious nanotubes' G and D bands for the composite fibers due to the minimal amounts used. X-ray photoelectron spectroscopy (XPS) was tried as an alternative method to identify the imperceptible information in these composite fibers. Fig. 4 shows the XPS spectra of C_{1s} of the composite fibers with 0, 0.4 and 0.8 wt% NH_2-MWCNTs, respectively. For neat PI fibers, four obvious peaks can be assigned to –C═O, –C–C, –C–O and –C–N groups, respectively. As shown in Fig. 4(B) and 4(C), upon adding NH_2-MWCNTs into PIs, a low and broad peak around 290.1 eV appears (enlarged image of the selected region), and this peak gradually upshifts to 290.5 eV for the composite fiber with 0.8 wt% nanotubes, which indicates the formation of π-π interaction of phenyl groups between PI and NH_2-MWCNTs. By

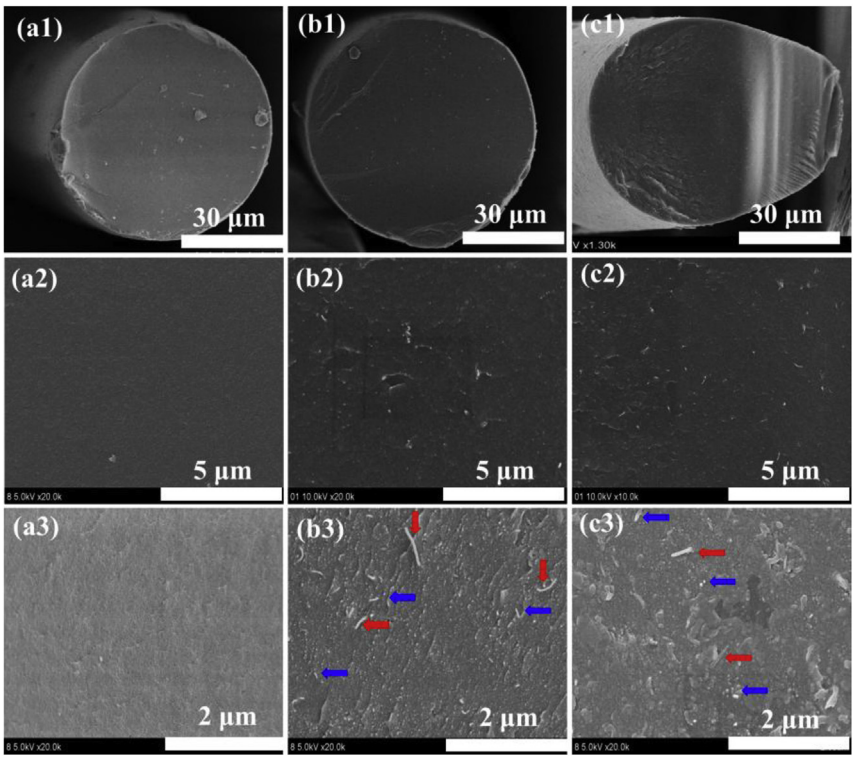

Fig. 2. SEM images of the cross-section morphology of the fracture surface for neat (a1, a2 and a3), PAA/0.4 wt% NH_2-MWCNTs composite fiber (b1, b2 and b3) and PAA/0.8 wt% NH_2-MWCNTs composite fiber (c1, c2 and c3).

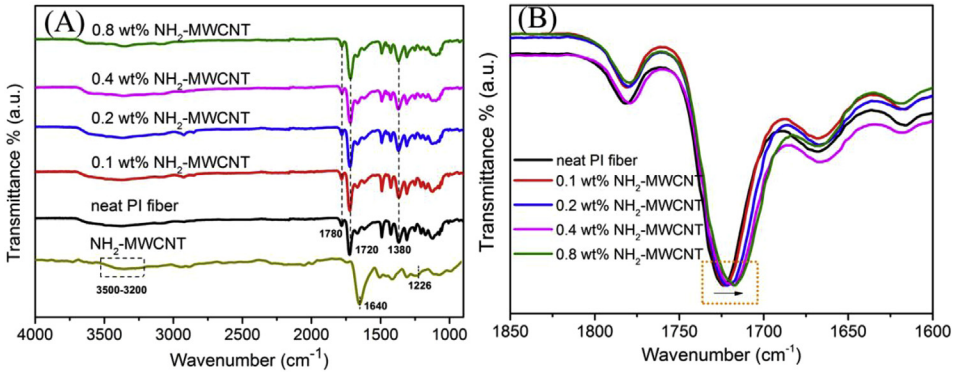

Fig. 3. FTIR spectra: (A) NH_2-MWCNT, neat-PI and PI/NH_2-MWCNTs composite fibers with various amounts of NH_2-MWCNTs; (B) PI/NH_2-MWCNTs composite fibers in the region of 1850–1600 cm^{-1}.

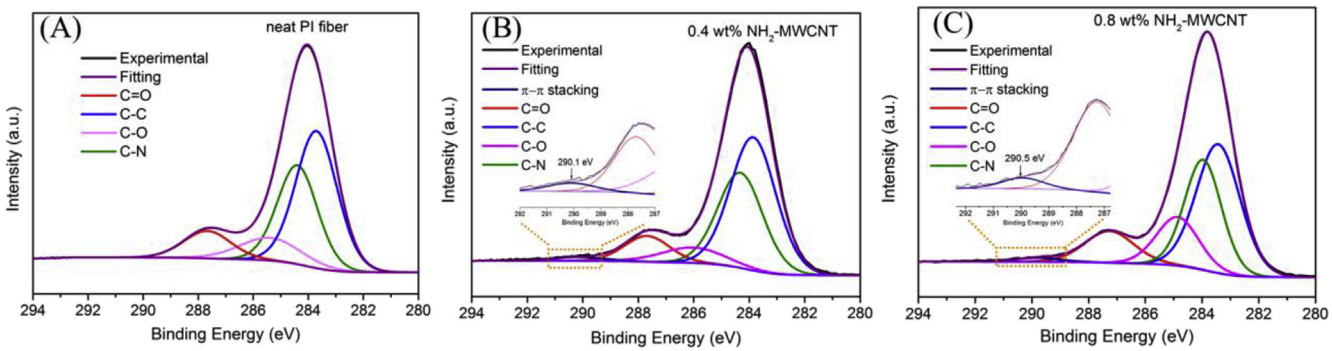

Fig. 4. XPS C_{1s} spectra of neat PI fiber (A) and (B, C) composite fibers with various loadings of NH_2-MWCNTs.

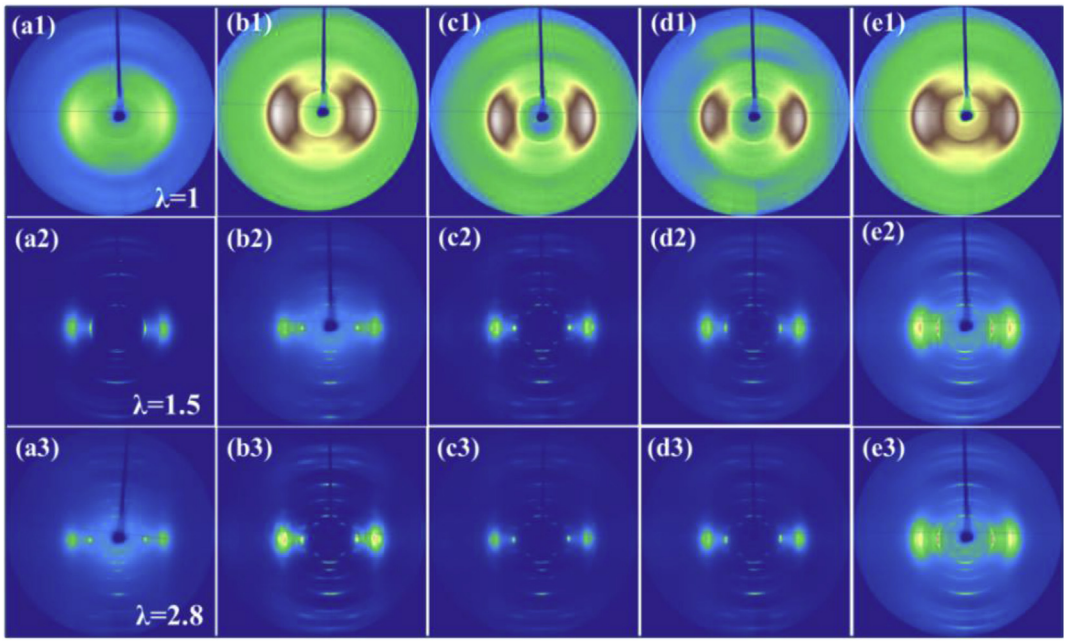

Fig. 5. WAXD patterns of the neat PI fiber and PI/NH_2-MWCNTs composite fibers with various nanotube loadings and draw ratios: (a) neat PI fiber, (b) 0.1 wt% NH_2-MWCNTs, (c) 0.2 wt% NH_2-MWCNTs, (d) 0.4 wt% NH_2-MWCNTs and (e) 0.8 wt% NH_2-MWCNTs.

means of UV–Vis spectra and Raman spectra, Wang and the co-workers also conformed the existence of π-π interaction between the MWCNTs and the 2,6-diaminoanthraquinone (a monomer for synthesising polyimide), which endows an excellent dispersibility and interfacial adhesion of MWCNTs in PIs [28]. Yuan's work shows the similar result that a rigid and unbent PAA backbone with biphenyl groups facilitate the stacking of dispersant molecules onto the conjugated MWCNTs surface *via* π-π interaction, promoting the long-term stability and individually dispersed MWCNTs [29].

Molecular orientation and crystallinity play important roles on the mechanical properties of the polymer fibers. In our previous work, the evolution of the aggregation structure of BPDA-BIA PI fibers has been investigated in detail [30]. The present study identified the changes of the structure of these composite fibers induced by the incorporation of amino-functionalized CNTs and estimated the nanotubes' impact on the structural and fibers' properties. Fig. 5 shows the WAXD patterns of the composite fibers with various amounts of NH_2-MWCNTs in dependence of the draw ratio. Obviously, the 2D intensity distributions of the neat PI and the PI/NH_2-MWCNTs composite fibers exhibit significant changes with increasing draw ratios, indicating the aggregation structure of these polymers responds quite sensitive to changes of processing conditions. Meanwhile, it is not difficult to find that these composite samples show better-defined intermolecular packing orders than the neat PI fiber when the draw ratio is over 1.5, suggesting the addition of nanotubes has influenced the microstructure of the polymer materials.

For details, 1D WAXD intensity profiles of the prepared fibers with $\lambda = 2.8$ in the equator and meridian are shown in Fig. 6. Along the equator, two diffraction peaks around $2\theta = 7.63°$ and 12.0° can be observed, and the diffraction intensities gradually increase with the NH_2-MWCNTs loadings up to 0.4 wt%. In addition, the diffraction peak at $2\theta = 7.63°$ ($d_{spacing} = 5.83$ nm) for the samples with the nanotube loadings less than 0.4 wt%, shifts to a lower location at $2\theta = 7.46°$ ($d_{spacing} = 5.96$ nm), indicating that the interplanar spacing of the semicrystal increases due to incorporating moderate amounts of NH_2-MWCNTs. The (*002*) graphitic peak around $2\theta = 26°$ corresponding to MWCNTs have not been observed. In meridian direction, all samples exhibit several Bragg diffraction streaks at $2\theta = 6.70°$, 8.69°, 10.98°, 14.75° and 20.88°,

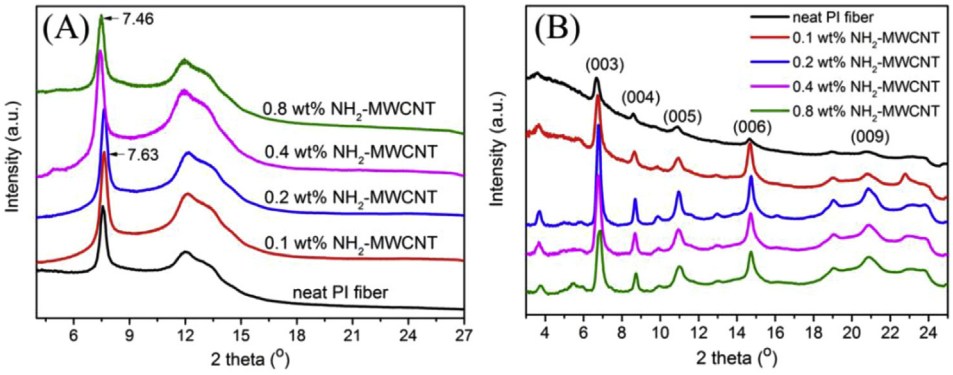

Fig. 6. One-dimensional integrated WAXD intensity profile of PI/NH_2-MWCNTs composite fibers with various NH_2-MWCNTs loadings at the draw ratio $\lambda = 2.8$: (A) equator; (B) meridian.

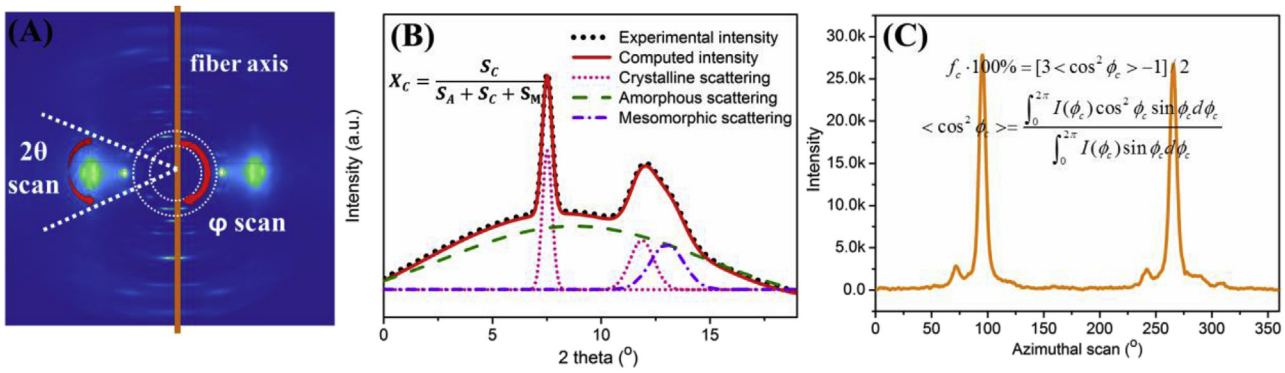

Fig. 7. Principle of the WAXD analysis shown for a PI/NH_2-MWCNTs composite fiber with the nanotube loading of 0.2 wt%. (A) Typical 2D WAXD pattern; (B) One-dimensional integrated WAXD intensity profile and the corresponding peak separation analysis to estimate the crystallinity; (C) Azimuthal ϕ scan around (003) Bragg reflection of the fiber.

corresponding to (003), (004), (005), (006) and (009) plane, respectively [30]. The scattering pattern along the meridian indicates a lamellar structure of (*00l*) plane stacking parallel to the fiber axis. The NH_2-MWCNTs have little effect on the lamellar structure of the drawn PI fibers. However, the chains orientation in the heat-drawing process has been influenced by these nanotubes as evidenced by the intensity increase of the diffraction peaks. The detailed values of orientation factor will be discussed in the following.

For analyzing the polymer structure of the composite fibers using WAXD, radical 2θ scans and azimuthal ϕ scan were carried out. Generally, as shown in Fig. 7(B), there coexist crystalline, amorphous and mesomorphic phases in polymers and curve-fitting deconvolution of the intensity profiles along the equator was performed using Peak-fit Software to separate various phase contributions. In order to quantitatively evaluate the degree of molecular orientation along the fiber axis, Hermans' orientation factor (f_c) was calculated based on the (*003*) plane, as shown in Fig. 7(C).

Fig. 8(A) shows the azimuthally integrated traces of the peak around $2\theta = 6.70^\circ$ for the neat PI and PI/NH_2-MWCNTs fibers with three different draw ratios. Obviously, the azimuthal intensity becomes stronger and the spreads tends to narrower with increasing the content of nanotubes up to 0.4 wt%. However, continue rising the content of NH_2-MWCNTs to 0.8 wt% results in broad and diffused integrated traces, implying a preferential chain orientation occurs for the samples with moderate amounts of NH_2-MWCNTs. Crystallinity and orientation of the neat PI and composite fibers are shown in Fig. 8(B). For the undrawn samples, the NH_2-MWCNTs concentration has little effect on the values of crystallinity and orientation; while, after the heat-drawing treatment, composite fibers show an increasing tendency in these two parameters. For the PI/NH_2-MWCNTs (0.4 wt%) sample with $\lambda = 2.8$, the values of crystallinity and Hermans' orientation reach 28.5% and 88.4%, respectively, which are 11.7% and 5.6% higher than the neat PI fiber. These results indicate that NH_2-MWCNTs are harmless or helpful for the packing and arrangement of PI molecular chains. The high aspect ratios of nanotubes make them susceptible to be stretched along the fiber axis during the spinning and post heat-drawing process, which is expected to the improved mechanical properties of the composite fibers.

The reinforcing effects of the amino-functionalized carbon nanotubes on the tensile properties of the PI composite fibers are summarized in Fig. 9. At the same draw ratio of $\lambda = 2.8$, the tensile strength of PI/NH_2-MWCNTs composites increases from 1.64 to 2.41 GPa (approximately a 47% increase over neat PI fiber), and the modulus increases from 72.24 to 99.0 GPa when increasing the content of NH_2-MWCNTs from 0.1 to 0.4 wt%, revealing that NH_2-MWCNTs possess a high reinforcing efficiency for promoting the load transfer from the polymer to the nanotubes. This increasing trend of tensile properties of the composite fibers can be attributed to the hydrogen-bonding and π-π interaction between PI matrix and NH_2-MWCNTs as well as the relatively higher crystallinity and

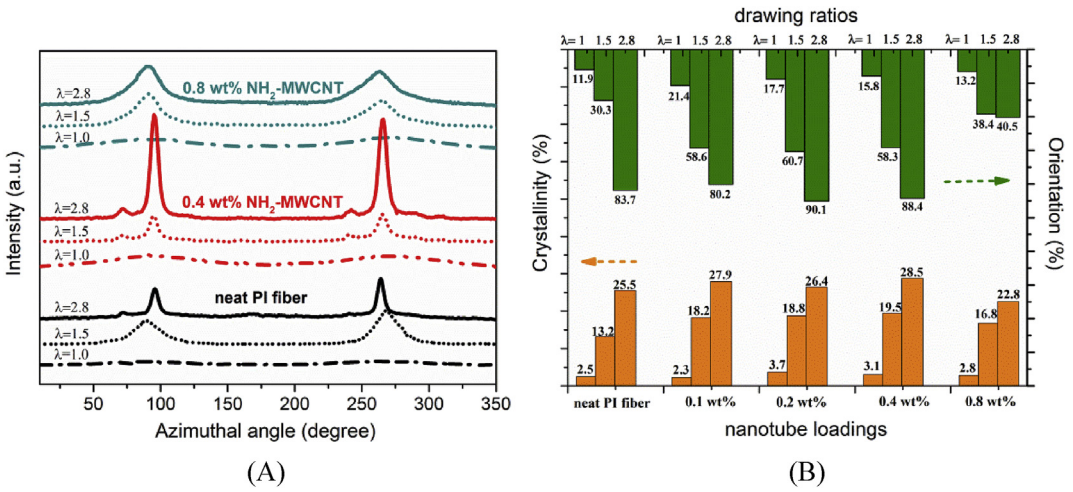

Fig. 8. (A) Azimuthal scans of neat PI and composite fibers with 0.4 wt% and 0.8 wt% NH_2-MWCNTs; (B) crystallinity and orientation factors of the neat PI and composite fibers as a function of the draw ratios.

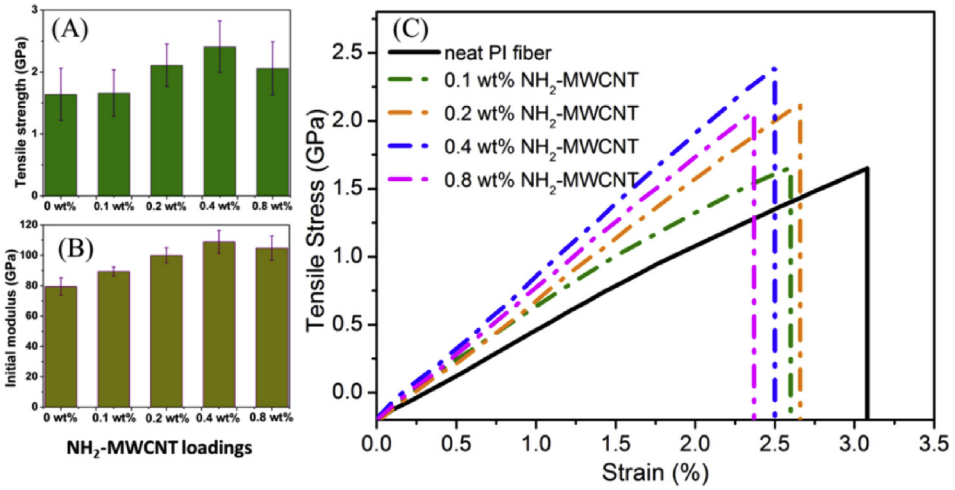

Fig. 9. (A) Tensile strength, (B) tensile modulus and (C) stress-strain curves of neat PI fiber and PI/NH_2-MWCNTs composite fibers with various amounts of NH_2-MWCNTs.

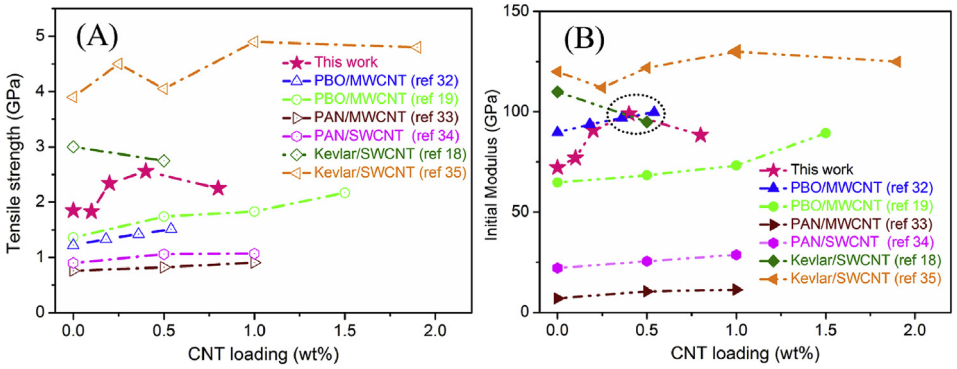

Fig. 10. Comparison of tensile strength (A) and initial modulus (B) of PI/NH_2-MWCNTs composite fibers in this study with published values for other polymer composite fibers. The tensile data for other composite fibers were reprinted from the noted reference.

molecules orientation of the composite fibers. However, a decreasing trend of tensile strength and modulus was observed as the nanotubes content increases from 0.4 to 0.8 wt%, which may be attributed to the filled NH_2-MWCNTs reaching a critical content. Xin and the coworkers called this critical point as *mechanical percolation* when they investigated the PVA/GO composites [31]. Lower than this content, the nanofillers (such as GO, CNT) can be well-dispersed in the polymer matrix, and the increase of loading has a significant improvement on the mechanical properties, while further loading may cause the nanofillers stacking together, weakening the efficiency of the mechanical improvement.

Fig. 10 further shows comparison of our tensile properties with the values reported in literature for other polymer/CNTs composite fibers. For most cases, the tensile strength and modulus of these composite fibers exhibit increasing trend when incorporating nanotubes. Our absolute tensile values at all nanotube loadings investigated are higher than the reported modulus and strength of PBO/CNT [19,32] and PAN/CNT systems [33,34], which set PI/NH_2-MWCNTs composite fibers among high-performance polymer fibers even though the tensile values are lower than the Kevlar/CNTs composite systems [18,35].

Considering the strong interaction between the PI matrix and

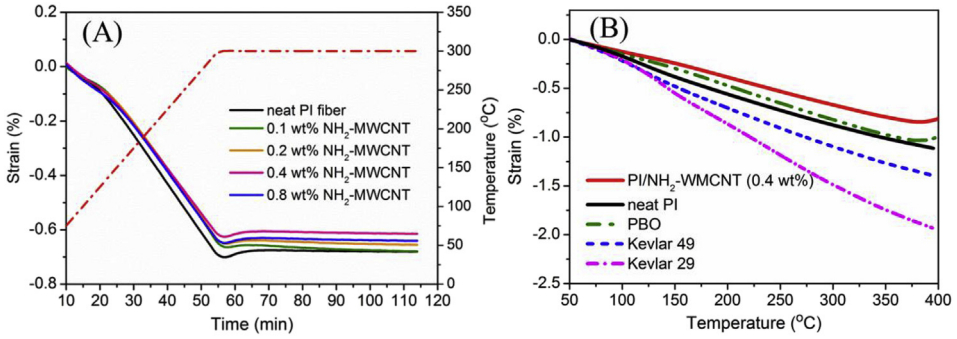

Fig. 11. (A) Change of the strain for PI/NH_2-MWCNTs composite fibers at a stress of 8 MPa; (B) strain change of neat PI, PI composite fiber, Kevlar fibers and PBO fiber during the heating process from 50 to 400 °C.

Table 1
Dimensional stability of the PI, PI composite fibers, Kevlar and PBO fiber.

Samples	Strain at 90 min (%)	Samples	Strain at 350 °C (%)
neat PI	−0.68	neat PI	−1.01
0.1 wt% NH_2-MWCNT	−0.67	PI/NH_2-MWCNT	−0.78
0.2 wt% NH_2-MWCNT	−0.63	PBO	−0.98
0.4 wt% NH_2-MWCNT	−0.60	Kevlar 29	−1.26
0.8 wt% NH_2-MWCNT	−0.62	Kevlar 49	−1.74

the NH_2-MWCNTs, we expect a substantial enhancement in thermal stability and thermal dynamical property of the composite fibers. As shown in Figs. S1 and S2 of the supplementary information, the maximum mass loss temperature (T_{max}) increases by 12 °C when adding 0.4 wt% NH_2-MWCNTs into PIs. Glass transition temperatures (T_gs, peak temperature of tan δ) of the composite fibers ranges from 360 °C to 367 °C. The thermal dimensional stability is of importance for the high performance polymeric fibers. Fig. 11(A) shows the changes in the strain of the PI/NH_2-MWCNTs composite fibers versus time during the heating process. All samples exhibit a heat shrinkage behavior when heated at a constant stress of 8 MPa. Up to the stable temperature of 300 °C, the corresponding strain values at 90 min for all these fibers are lower than 0.7%. The composite fiber containing 0.4 wt% NH_2-MWCNTs shows the lowest strain, which is almost 1% lower than the neat PI fiber, representing enhancement effect of NH_2-MWCNTs on the thermal dimensional stability of the composite fibers. We further compared the thermal dimensional stabilities of the PI/NH_2-MWCNTs composite fiber with Kevlar and PBO fibers, as shown in Fig. 11(B). In the heating process, Kevlar 29 and Kevlar 49 show obvious changes in the strain, and the neat PI and PBO fibers exhibit a similar dimensional change behavior. These differences can be explained by the different rigidities of the molecular chains. Furthermore, in Table 1, the strain values of the PI/NH_2-MWCNTs composite fiber show a reduced tendency compared to other samples, which are mainly attributed to the rigid structure and good dispersion of the CNTs in the PI matrix.

4. Conclusions

We successfully fabricated PI/NH_2-MWCNTs composite fibers with enhanced mechanical properties and dimension stabilities. Utilizing the NH_2-MWCNTs/NMP suspension is beneficial for ensuring excellent dispersivity and good compatibility of CNTs in polymer matrix. The reinforcing effects of these 1D cylindrical fillers was implemented by the multiple interfacial interactions between PI and CNTs as well as the facilitating roles of CNTs on the crystallinity and polymer chains orientation of the PI matrix. The PI/NH_2-MWCNTs composite fibers with only 0.4 wt% NH_2-MWCNTs content showed a 47% increase in tensile strength and 27% improvement in modulus. These results in this work show a great potential application in fabricating CNT-based PI composite fibers, and may be applied in industrial production.

Acknowledgements

This work was supported by National Natural Science Foundation of China (No. 51233001), 973 plan (2014CB643603). Thanks to SSRF for the WAXD measurement and discussion.

Appendix A. Supplementary data

Supplementary data related to this article can be found at http://dx.doi.org/10.1016/j.compscitech.2016.09.021.

References

[1] S.Z. Cheng, Z. Wu, E. Mark, A high-performance aromatic polyimide fibre: 1. Structure, properties and mechanical-history dependence, Polymer 32 (10) (1991) 1803–1810.
[2] M. Eashoo, D. Shen, Z. Wu, C.J. Lee, F.W. Harris, S.Z. Cheng, High-performance aromatic polyimide fibres: 2. Thermal mechanical and dynamic properties, Polymer 34 (15) (1993) 3209–3215.
[3] J. Dong, C. Yin, W. Luo, Q. Zhang, Synthesis of organ-soluble copolyimides by one-step polymerization and fabrication of high performance fibers, J. Mater. Sci. 48 (21) (2013) 7594–7602.
[4] T. Sukhanova, Y.G. Baklagina, V. Kudryavtsev, T. Maricheva, F. Lednický, Morphology, deformation and failure behaviour of homo-and copolyimide fibres: 1. Fibres from 4, 4′-oxybis (phthalic anhydride)(DPhO) and p-phenylenediamine (PPh) or/and 2, 5-bis (4-aminophenyl)-pyrimidine (2, 5PRM), Polymer 40 (23) (1999) 6265–6276.
[5] H. Niu, M. Huang, S. Qi, E. Han, G. Tian, X. Wang, et al., High-performance copolyimide fibers containing quinazolinone moiety: preparation, structure and properties, Polymer 54 (6) (2013) 1700–1708.
[6] J. Dong, C. Yin, X. Zhao, Y. Li, Q. Zhang, High strength polyimide fibers with functionalized graphene, Polymer 54 (23) (2013) 6415–6424.
[7] C. Yin, J. Dong, Z. Li, Z. Zhang, Q. Zhang, Large-scale fabrication of polyimide fibers containing functionalized multiwalled carbon nanotubes via wet spinning, Compos. Part. B Eng. 58 (2014) 430–437.
[8] D. Chen, R. Wang, W.W. Tjiu, T. Liu, High performance polyimide composite films prepared by homogeneity reinforcement of electrospun nanofibers, Compos. Sci. Technol. 71 (13) (2011) 1556–1562.
[9] C. Zhou, R. Chu, R. Wu, Q. Wu, Electrospun polyethylene oxide/cellulose nanocrystal composite nanofibrous mats with homogeneous and heterogeneous microstructures, Biomacromolecules 12 (7) (2011) 2617–2625.
[10] Z. Xu, C. Gao, *In situ* polymerization approach to graphene-reinforced nylon-6 composites, Macromolecules 43 (16) (2010) 6716–6723.
[11] X. Zhang, Q. Li, T.G. Holesinger, P.N. Arendt, J. Huang, P.D. Kirven, et al., Ultrastrong, stiff, and lightweight Carbon-nanotube fibers, Adv. Mater. 19 (23) (2007) 4198–4201.
[12] J. Huang, X. Li, L. Luo, H. Wang, X. Wang, K. Li, et al., Releasing silica-confined macromolecular crystallization to enhance mechanical properties of polyimide/silica hybrid fibers, Compos. Sci. Technol. 101 (2014) 24–31.
[13] T.W. Chou, L. Gao, E.T. Thostenson, Z. Zhang, J.H. Byun, An assessment of the science and technology of carbon nanotube-based fibers and composites, Compos. Sci. Technol. 70 (1) (2010) 1–19.
[14] H.G. Chae, T. Sreekumar, T. Uchida, S. Kumar, A comparison of reinforcement efficiency of various types of carbon nanotubes in polyacrylonitrile fiber, Polymer 46 (24) (2005) 10925–10935.
[15] J. Zhu, W. Cao, M. Yue, Y. Hou, J. Han, M. Yang, Strong and stiff aramid nanofiber/carbon nanotube nanocomposites, ACS Nano 9 (3) (2015) 2489–2501.
[16] K. Song, Y. Zhang, J. Meng, E.C. Green, N. Tajaddod, H. Li, et al., Structural polymer-based carbon nanotube composite fibers: understanding the processing-structure-performance relationship, Materials 6 (6) (2013) 2543–2577.
[17] T. Vad, J. Wulfhorst, T.T. Pan, W. Steinmann, S. Dabringhaus, M. Beckers, et al., Orientation of well-dispersed multiwalled carbon nanotubes in melt-spun polymer fibers and its impact on the formation of the semicrystalline polymer structure: a combined wide-angle X-ray scattering and electron tomography study, Macromolecules 46 (14) (2013) 5604–5613.
[18] L. Deng, R.J. Young, S. van der Zwaag, S. Picken, Characterization of the adhesion of single-walled carbon nanotubes in poly (p-phenylene terephthalamide) composite fibres, Polymer 51 (9) (2010) 2033–2039.
[19] Z. Hu, J. Li, P. Tang, D. Li, Y. Song, Y. Li, et al., One-pot preparation and continuous spinning of carbon nanotube/poly (p-phenylene benzobisoxazole) copolymer fibers, J. Mater. Chem. 22 (37) (2012) 19863–19871.
[20] T. Sainsbury, K. Erickson, D. Okawa, C.S. Zonte, J.M. Fréchet, A. Zettl, Kevlar functionalized carbon nanotubes for next-generation composites, Chem. Mater. 22 (6) (2010) 2164–2171.
[21] X. Liu, G. Gao, L. Dong, G. Ye, Y. Gu, Correlation between hydrogen-bonding interaction and mechanical properties of polyimide fibers, Polym. Adv. Technol. 20 (4) (2009) 362–366.
[22] S. Ran, D. Fang, X. Zong, B. Hsiao, B. Chu, P. Cunniff, Structural changes during deformation of kevlar fibers *via* on-line synchrotron SAXS/WAXD techniques, Polymer 42 (4) (2001) 1601–1612.

[23] S.S. Rahatekar, A. Rasheed, R. Jain, M. Zammarano, K.K. Koziol, A.H. Windle, et al., Solution spinning of cellulose carbon nanotube composites using room temperature ionic liquids, Polymer 50 (19) (2009) 4577–4583.
[24] T. Ramanathan, F. Fisher, R. Ruoff, L. Brinson, Amino-functionalized carbon nanotubes for binding to polymers and biological systems, Chem. Mater. 17 (6) (2005) 1290–1295.
[25] Y. Wang, Z. Shi, J. Fang, H. Xu, J. Yin, Graphene oxide/polybenzimidazole composites fabricated by a solvent-exchange method, Carbon 49 (4) (2011) 1199–1207.
[26] T.K. Ahn, M. Kim, S. Choe, Hydrogen-bonding strength in the blends of polybenzimidazole with BTDA-and DSDA-based polyimides, Macromolecules 30 (11) (1997) 3369–3374.
[27] J. Dong, C. Yin, Z. Zhang, et al., Hydrogen-bonding interactions and molecular packing in polyimide fibers containing benzimidazole units, Macromolecular. Mater. Eng. 299 (10) (2014) 1170–1179.
[28] N. Wang, et al., *In situ* preparation of reinforced polyimide nanocomposites with the noncovalently dispersed and matrix compatible MWCNTs, Compos. Part A Appl. S 78 (2015) 341–349.
[29] W. Yuan, J. Che, M.B. Chan-Park, A novel polyimide dispersing matrix for highly electrically conductive solution-cast carbon nanotube-based composite, Chem. Mater. 23 (18) (2011) 4149–4157.
[30] C. Yin, J. Dong, W. Tan, J. Lin, D. Chen, Q. Zhang, Strain-induced crystallization of polyimide fibers containing 2-(4-aminophenyl)-5-aminobenzimidazole moiety, Polymer 75 (2015) 178–186.
[31] X. Zhao, Q. Zhang, D. Chen, P. Lu, Enhanced mechanical properties of graphene-based poly(vinyl alcohol) composites, Macromolecules 43 (5) (2010) 2357–2363.
[32] C. Zhou, S. Wang, Y. Zhang, Q. Zhuang, Z. Han, *In situ* preparation and continuous fiber spinning of poly (p-phenylene benzobisoxazole) composites with oligo-hydroxyamide-functionalized multi-walled carbon nanotubes, Polymer 49 (10) (2008) 2520–2530.
[33] J. Zhang, Y. Zhang, D. Zhang, J. Zhao, Dryjet wet-spun PAN/MWCNT composite fibers with homogeneous structure and circular cross-section, J. Appl. Polym. Sci. 125 (S1) (2012).
[34] H.G. Chae, M.L. Minus, S. Kumar, Oriented and exfoliated single wall carbon nanotubes in polyacrylonitrile, Polymer 47 (10) (2006) 3494–3504.
[35] I. O'Connor, H. Hayden, J.N. Coleman, Y.K. Gun'ko, High-Strength, high-toughness composite fibers by swelling kevlar in nanotube suspensions, Small 5 (4) (2009) 466–469.